# Highly directive Fabry-Perot leaky-wave nanoantennas based on optical partially reflective surfaces

# Highly directive Fabry-Perot Leaky-Wave nanoantennas based on optical Partially Reflective Surfaces

M. Lorente-Crespo[1] and C. Mateo-Segura[1, a)]
*Institute of Sensors, Signals and Systems, Heriot-Watt University, EH14 4AS, Edinburgh, UK*

(Dated: 23 March 2015)

Nanoantennas enhance the conversion between highly localized electromagnetic fields and far-field radiation. Here, we investigate the response of a nano-patch Partially Reflective Surface backed with a silver mirror to an optical source embedded at the centre of the structure. Using full wave simulations, we demonstrate a two orders of magnitude increased directivity compared to the isotropic radiator, 50% power confinement to a $13.8^o$ width beam and a $\pm 16$ nm bandwidth. Our antenna does not rely on plasmonic phenomena thus reducing non-radiative losses and conserving source coherence.

During the last decades, nanotechnology has made a significant breakthrough in the development of novel optoelectronic devices allowing the accurate fabrication and integration of nanocomponents in flexible and inexpensive materials.[1] The resulting nanodevices have had tremendous impact in optical communication, sensing, imaging and photovoltaic systems.[2–4] In the latter, the ability to enhance, confine, receive, and transmit optical fields, which are known basic functions of antennas, is required. Hence, the study of nanoantennas has become the subject of intensive research and a rapidly growing field of nanoscience. Nanoantennas are devices capable of connecting free-space far-field radiation and nanoscale optical signals. Their design methodology resembles that of its radio-frequency (RF) counterparts where its properties can be tailored to fulfill a specific function. However, conventional rules for light-matter interaction need to be re-examined to fit the different phenomena involved. One of the major differences is a dramatic change in behavior of metals which cannot be treated as (nearly) perfect conductors. Their optical response is described instead by a frequency-dependent complex dielectric function associated with material losses and non-negligible field penetration.[5] In addition, surface plasmon polaritons may be excited. Many designs inspired by well-established RF antennas can be found in the literature. This is the case of: monopoles,[6] dipoles,[4,7] patch-antennas[8,9] and more interestingly arrays of these elements (e.g. Yagi-Udas[10,11]). Nanoantenna arrays offer additional degrees of freedom for tailoring the radiation pattern such as the geometry of the individual elements, their relative positions, orientations and density; which makes them especially promising for spontaneous emission enhancement, solar energy harvesting, 3D holography displays and enhancement of photodetectivity of infrared detectors.[11–14]

In this context, we introduce a miniaturized Leaky Wave (LW) antenna operating in the near-infrared (NIR) offering up to 21.2 dBi directivity at broadside with a $13.8^o$ beamwidth. The fractional bandwidth, defined as the frequency range for which the radiated power decays less than 50% of its maximum value normalized to the central frequency, is 2.8%. LW antennas have been extensively used to tailor the radiation pattern of low directive sources in the microwave regime. They are capable of concentrating the radiated power into highly directive pencil-beams at the frequency of operation and conical beams above it.[15] A common type of 2-D LW antenna consists of a Partially Reflecting Surface (PRS) over a ground plane (GP) forming a half-wavelength Fabry-Pérot cavity. The cavity is excited by a horizontal hertzian electric dipole located at its center. At optical frequencies, such a source may consist in practice of a stimulated molecule or an embedded quantum dot. The periodic set of perturbations provided by the highly reflective PRS allow the radiation to leak out, while the GP reflects all the incident power, avoiding power lost in the backward direction. As a result, multiple reflections appear inside the half-wavelength cavity which at the operating frequency of the antenna are in phase at the PRS plane and transmitted waves constructively interfere towards radiation.[16]

A PRS consisting of an infinite grating of square silver nanopatches with thickness $t = 20$ nm and side $l = 200$ nm arranged in a 2D square lattice with periodicity $a = 250$ nm [Fig 1(a)] is considered. The dielectric function of silver is described using Drude's model with plasma frequency $\omega_p = 1.39 \times 10^{16}$ rad/s and damping frequency $\Gamma = 5.13$ THz.[17] The angular reflectivity spectra shows a maximum at about 300 THz for transverse-magnetic (TM) and transverse-electric (TE) polarized incident waves [Figs. 1(b) and 1(c), respectively]. At oblique incidence some important differences between the TM and TE spectra can be observed. For a TM polarized wave [Fig. 1(b)], a vertical band with almost zero reflectivity arises between 50 and 260 THz that is not present for TE polarization. This broadband extraordinary transmission effect has been attributed to anomalous perfect impedance matching of the impinging electromagnetic radiation at the plasmonic Brewster's angle in optical plasmonic gratings and can be predicted using a transmission line model (TLM).[18] The condi-

a)Electronic mail: C.Mateo-Segura@hw.ac.uk

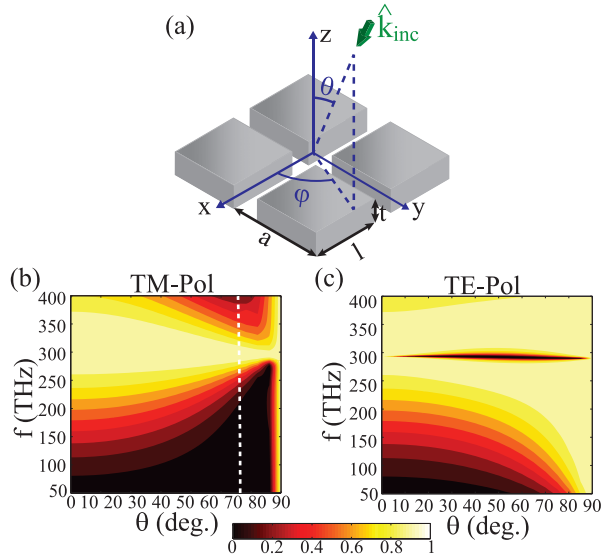


FIG. 1. (color online). (a) Proposed PRS. (b)-(c) Angular reflection spectra of a PRS with $l = 200$ nm, $a = 250$ nm and $t = 20$ nm at $\varphi = 0^o$, $90^o$ for a (b) TM- and a (c) TE-polarized wave. The plasmonic Brewster's angle is indicated with a white dashed line.

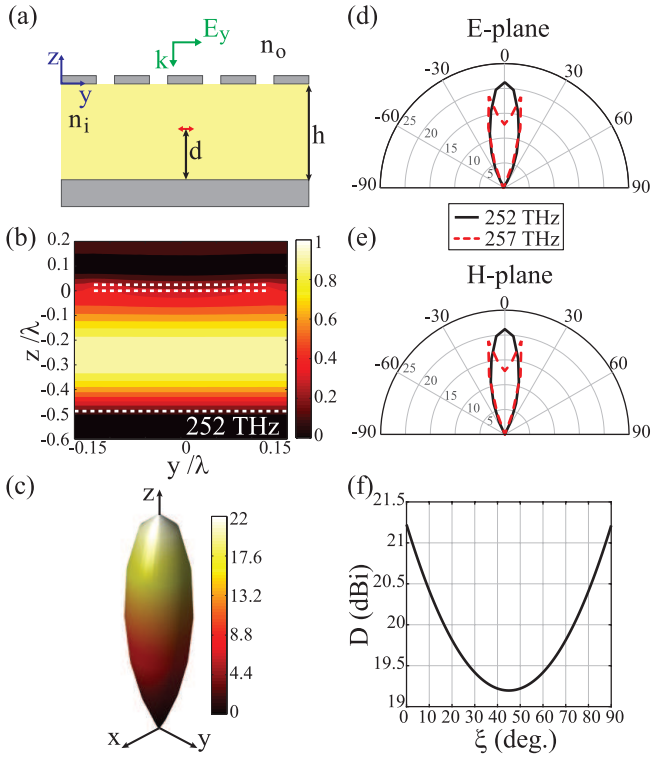


FIG. 2. (color online). (a) Side view of the LW nanoantenna. The horizontal optical source is shown with a red arrow. (b) Normalized E-field distribution at normal incidence. The position of a nanopatch and the GP are indicated with dashed white lines. (c) 3D-Directivity pattern (dBi) of the nanoantenna. (d)-(e) Directivity pattern at the (d) E- and (e) H-plane. (f) Directivity at broadside when the source is oriented at an angle from the y-axis.

tion for anomalous perfect matching is independent of the thickness of the grating, provided that it is optically thick enough. In our case, the metal particles are thinner than the skin depth allowing the incident E-field to penetrate into the metal while suffering very little absorption. As a result, transmission occurs not only through the gaps between adjacent nanopatches but also through the nanoparticles causing the angle of minimum reflectivity to appear deviated from that predicted by the TLM which is indicated by a dashed line in Fig. 1(b). When the wave impinging the PRS is TE polarized, a horizontal narrow band of zero reflectivity is observed [Fig. 1(c)]. This wide-angle resonance is originated by the excitation of a localized surface plasmon which splits the reflectivity maximum.[19]

The LW nanoantenna is formed by locating a sufficiently thick silver GP at $h = 398$ nm ($\sim\lambda/2$) from the PRS. Unless otherwise stated, the nanoantenna is completely embedded in silica, $n_i = n_o = 1.45$, in order to avoid any mismatch effect. The inhomogeneous case, $n_i \neq n_o$, will be discussed later in this Letter. The magnitude of the reflection coefficient of the PRS determines the maximum directivity of the nanoantenna while the pointing angle is related to its phase.[16] The height of the cavity $h$ is slightly shorter than that expected from traditional antenna design due to the non-negligible field penetration into the metal.[20] A y-directed optical source emitting at 252 THz is placed at the center of the cavity formed [Fig. 2(a)]. Such a source emits electromagnetic waves as either $TM_z$ or $TE_z$ which determine the E- and H-planes of the antenna, respectively.[21] Our simulations show that the position of the source along the XY plane has very little effect on the radiation pattern, in contrast to its vertical position [Fig. 2(b)]. Here, a perturbed version of the TM/TE first order mode of the corresponding parallel plate cavity is observed upon excitation of the source. At the frequency of operation, a standing wave in the transverse direction is formed, being the field maximum at $d \sim h/2$. The separation from the embedded source to the free surfaces is sufficient to avoid non-radiative recombinations associated with surface states thus conserving source coherence.[22]

The performance of the LW nanoantenna is analyzed using CST Microwave Studio together with reciprocity. According to the reciprocity theorem, the receiving pattern of an antenna equals that of its transmission pattern. Therefore, assuming a y-directed optical source at $d$, the problem of calculating the far-field radiated by the LW nanoantenna reduces to sampling the y-component of the electric near-field at the source position when a plane-wave impinges from any angle of incidence $(\theta, \varphi)$. The 3D directivity pattern [Fig. 2(c)] is then obtained as the ratio of the radiation intensity in each direction and the power emitted by the nanoantenna over the whole space[23]. As expected, a highly directive narrow pencil beam with $13.8^o$ 3dB-angular width is obtained at the

frequency of operation of the nanoantenna instead of the dipole characteristic toroidal pattern. The directivity at broadside ($\theta = 0^o$) is 21.2 dBi. TM-polarized waves impinging at the angle of minimum reflection [Fig. 1(b)] will essentially contribute to the z-component of the E-field to which a horizontal source cannot couple. As a result, no side-lobes are observed regardless of the reflection minimum in the angular spectra. However, it is worth mentioning that for those sources in which the z-component plays an active role, for instance a vertical dipole, radiation at the plasmonic Brewster's angle should be expected. On the other hand, the wide-angle zero reflectivity band in the TE-polarization response of the PRS [Fig. 1(c)] appears above the operating frequency of the nano-antenna, not affecting its performance. The directivity patterns at E- and H-planes ($\varphi = 90^o$ and $\varphi = 0^o$, respectively) for two different frequencies [Figs. 2(d) and 2(e)] are nearly symmetrical. As a result of increasing the operating frequency, or equivalently employing higher cavities, the resonant condition of the cavity is fulfilled at oblique incidence. Consequently, the pointing angle increases and the pencil beam turns into a conical beam. This effect is shown with dashed red lines in Figs. 2(d) and 2(e). Due to the nature of the sources needed to excite this antennas, a precise control on their orientation in the XY-plane is extremely challenging. Fig. 2(e) shows that the directivity at broadside varies less than 2 dB when the source is rotated an angle $\xi$ with respect to the y-axis, i.e. it is barely affected by orientation changes.

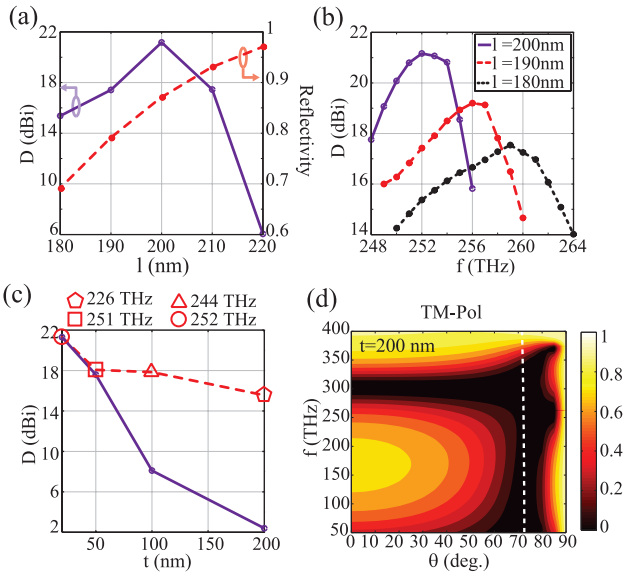


FIG. 3. (color online). (a) Directivity at broadside (right axis) and PRS reflectivity (left axis) when $a = 250$ nm, $t = 20$ nm, $h = 398$ nm and $l = 180 - 220$ nm. (b)-(c) Directivity at broadside when: (b) $l = 180 - 200$ nm and (c) $t = 20 - 200$ nm. The purple solid line in (c) is the directivity at 252 THz and the red dashed line at the frequencies at which the pencil beam is obtained (indicated in the legend). (d) TM Angular reflectivity spectra when $t = 200$ nm. The plasmonic Brewster's angle is shown with a white dashed line.

To gain a better understanding of the performance of the nanoantenna, a parametric study of the PRS geometry was performed [Fig. 3]. The effect of varying the dimensions of the nanopatches is investigated and presented in Figs. 3(a) and 3(b) for a periodicity $a = 250$ nm. Silver's inherent losses are very low in this frequency range. Therefore, larger nanopatches produce more reflective PRSs while barely increasing the absorption [Fig. 3(a)] which in turn results in higher values of directivity. For $l = 200$ nm the directivity at broadside is maximized. For larger values of $l$, the gaps between adjacent nanopatches are significantly reduced. As a result, the operating frequency of the nano-antenna is red-shifted. At higher frequencies, constructive interference is achieved at angles different from broadside, resulting in the beam splitting. Fig. 3(b) shows the directivity at broadside for $l = 180, 190$ and 200 nm. As a consequence of increasing the size of the nanopatches up to the optimum ($l = 200$ nm) the 3dB-fractional bandwidth is reduced. The coupling of the cavity to the incoming plane wave decreases resulting in higher external quality factors and thus lower 3dB-fractional bandwidths. In particular, for $l = 200$ nm the 3dB-bandwidth is 2.8% for a central frequency of 252 THz while for $l = 190$ nm and $l = 180$ nm it is 3.7% and 5.1%, respectively. In conclusion, there is a tradeoff between directivity and bandwidth. The periodicity also plays a key role in the performance of the nanoantenna. As long as the period is below the first Bragg resonance, such as the case presented in this Letter, only the zeroth diffraction order is radiated. Thus, the effect of varying the periodicity within this range (not shown here for the sake of brevity) can be understood as complementary of that obtained when changing the dimensions of the nanopatches. The optimum periodicity was found to be $a = 250$ nm.

Typically, when designing LW antennas in the microwave regime, metals are assumed to be good conductors with negligible thickness. This assumption is not valid at the frequency range at hand. Furthermore, the effective height of the cavity depends on the field penetration and hence, on the thickness of the nanopatches. The effect of the thickness of the metallic nanopatches in the nanoantenna radiation performance is studied in Fig. 3(c). The solid line shows the directivity at broadside at 252 THz for a given cavity height. For $t \neq 20$ nm the radiation pattern has a conical shape since the nanoantenna is not tuned to the operating frequency. The dashed line shows the directivity at the frequency at which the pencil beam is obtained for the different thicknesses indicated in the figure. For thicker nanopatches, the operating frequency is red-shifted. When the grating is sufficiently thick, i.e. the nanopatches are thicker than the penetration distance, the power is only transmitted through the gaps, diminishing the directivity. Since the field penetration which was not accounted for in the TLM is negligible in this situation, the angle of minimum reflectivity and the plasmonic Brewster's angle calculated

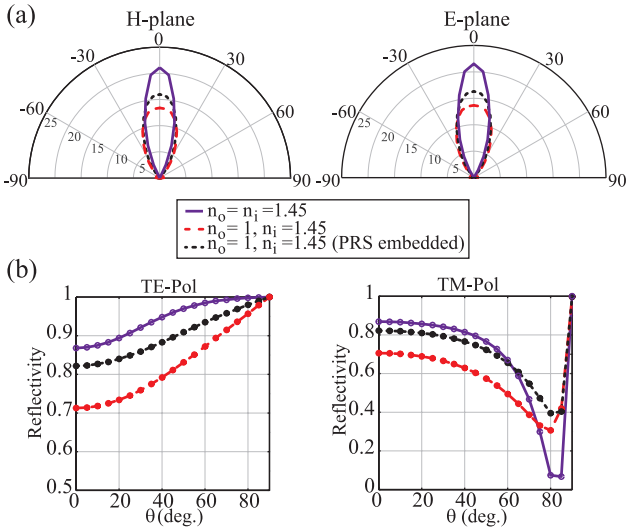


FIG. 4. (color online). (a) Directivity pattern (dBi) at the E- and H-plane when $n_i \neq n_o$ and the PRS lies on top of the silica slab at 266 THz (red dashed line), and when embedded at 259 THz (black dotted line). The homogeneous case (purple solid line) is included for comparison. (b) PRS's angular reflectivity spectra for both incoming polarizations.

using the TLM agree excellently [Fig. 3(d)].

A more practical scenario may consist of a LW nanoantenna surrounded by an inhomogeneous dielectric medium so that the power radiated by the nanoantenna couples to free-space. In this case, the PRS is assumed to lay on a dielectric media with refractive index $n_i$ while the surrounding space is vacuum. This situation is illustrated in Fig. 4(a) for two cases namely a PRS laying on top of a silica slab and a PRS embedded in silica. The dimensions of the nanoantenna are equal to those indicated in Figs. 1 and 2. For the sake of comparison, the LW nanoantenna pattern for $n_i = n_o = 1.45$ is also included. The effect of the index mismatch results in a reduced directivity, increased beam-width and a blue-shift of the operating frequency. This can be explained by looking at the angular reflection spectra of the PRS in Fig. 4(b). The reflectance at normal incidence is much lower than that of the homogeneous media. As a consequence, the directivity is reduced by 8 dB. The performance can be moderately improved with the embedded PRS which shows a directivity of 16 dBi. Other techniques such as employing gradient index substrates may further enhance the directivity.[24]

In conclusion, we have shown that 2D-periodic FP cavity type LW nanoantennas can control the far-field emission of optical sources. They are capable of tailoring the radiation pattern of low directive emitters into very narrow highly-directive pencil beams. Its planar nature may ease its integration with slab embedded sources. In preparation for an experimental realization, we have also considered the case in which the nanoantenna is embedded in an inhomogeneous substrate. Our results show that in this scenario, the nanoantenna still offers a very good performance. In addition, the nanoantenna does not rely on plasmonic effects, with the advantage of reduced non-radiative losses and higher separation to metallic parts than previously reported designs.[9] Such a device could find many exciting applications in the field of quantum communications and quantum cryptography. Despite the fractional bandwidth being small for the antenna to be considered broadband, a bandwidth of just a few THz is still enough for a broad variety of applications. Moreover, the bandwidth might be improved using similar techniques to those applied at microwaves.[23] Further investigation in this direction may be promising.

## ACKNOWLEDGMENTS

The authors would like to thank G. C. Ballesteros for valuable suggestions and to acknowledge the funding support by FP7 project DORADA (IAPP-2013-610691).

[1] G. Eda, G. Fanchini, and M. Chhowalla, Nature Nanotech. **3**, 270 (2008).
[2] A. Alù and N. Engheta, Phys. Rev. Lett. **104**, 213902 (2010).
[3] H. A. Atwater and A. Polman, Nature Mater. **9**, 205 (2010).
[4] L. Neumann, J. van 't Oever, and N. F. van Hulst, Nano Lett. **13**, 5070 (2013).
[5] S. A. Maier, *Plasmonics: Fundamentals and Applications* (Springer, 2007).
[6] T. H. Taminiau, F. D. Stefani, and N. F. van Hulst, New J. Phys. **10**, 105005 (2008).
[7] T. H. Taminiau, F. D. Stefani, F. B. Segerink, and N. F. van Hulst, Nature Photon. **2**, 234 (2008).
[8] C. Belacel, B. Habert, F. Bigourdan, F. Marquier, J.-P. Hugonin, S. M. de Vasconcellos, X. Lafosse, L. Coolen, C. Schwob, C. Javaux, B. Dubertret, J.-J. Greffet, P. Senellart, and A. Maitre, Nano Lett. **13**, 1516 (2013).
[9] R. Esteban, T. V. Teperik, and J. J. Greffet, Phys. Rev. Lett. **104**, 026802 (2010).
[10] D. Dregely, R. Taubert, J. Dorfmüller, R. Vogelgesang, K. Kern, and H. Giessen, Nat. Commun. **2**, 267 (2011).
[11] T. H. Taminiau, F. D. Stefani, and N. F. van Hulst, Opt. Express **16**, 10858 (2008).
[12] L. Cao, P. Fan, A. P. Vasudev, J. S. White, Z. Yu, W. Cai, J. A. Schuller, S. Fan, and M. L. Brongersma, Nano Lett. **10**, 439 (2010).
[13] Y. Yifat, M. Eitan, Z. Iluz, Y. Hanein, A. Boag, and J. Scheuer, Nano Lett. **14**, 2485 (2014).
[14] A. Bonakdar and H. Mohseni, Nanoscale **6**, 10961 (2014).
[15] T. Zhao, D. Jackson, J. Williams, H.-Y. D. Yand, and A. Oliner, IEEE Trans. Antennas Propag. **53**, 3505 (2005).
[16] G. Trentini, IRE Trans. Antennas Propag. **4**, 666 (1956).
[17] P. Johnson and R. Christy, Phys. Rev. B **6**, 4370 (1972).
[18] C. Argyropoulos, G. D'Aguanno, N. Mattiucci, N. Akozbek, M. J. Bloemer, and A. Alù, Phys. Rev. B **85**, 024304 (2012).
[19] J. Parsons, E. Hendry, J. R. Sambles, and W. L. Barnes, Phys. Rev. B **80**, 245117 (2009).
[20] L. Novotny, Phys. Rev. Lett. **98**, 1 (2007).
[21] A. Ip and D. Jackson, IEEE Trans. Antennas Propag. **38**, 482 (1990).
[22] J. Johansen, S. Stobbe, I. Nikolaev, T. Lund-Hansen, P. Kristensen, J. Hvam, W. Vos, and P. Lodahl, Phys. Rev. B **77** (2008), 10.1103/PhysRevB.77.073303.
[23] C. Mateo-Segura, A. Feresidis, and G. Goussetis, IEEE Trans. Antennas Propag. **62**, 586 (2014).
[24] N. T. Nguyen, R. Sauleau, and C. J. Martínez Pérez, IEEE Trans. Antennas Propag. **57**, 1907 (2009).